*Progress In Electromagnetics Research C, Vol. 105, 73–84, 2020*

# A Dual Circularly Reconfigurable Polarization Patch Antenna for Fifth Generation Mobile Communication Systems

**Nazih K. Mallat[1, *], Mahdi Nouri[2], Sajjad A. Aghdam[3], Muhammad T. Zia[4], Bassam Harb[1], and Alireza Jafarieh[5]**

**Abstract**—In this paper, a reconfigurable patch antenna with Circular Polarization (CP) diversity with theoretical discussion and verification is proposed for fifth generation (5G) of mobile communication systems. The proposed antenna contains two PIN diodes, which are correctly placed on the ground plane to obtain polarization diversity. By switching between two ON/OFF modes in the PIN diodes, the proposed antenna can support either the RHCP mode or the LHCP mode. An antenna with the well-matched impedance bandwidths ($S_{11} \leq -10\,\text{dB}$) of 2.5 GHz (27 $\sim$ 29.5 GHz) and 3 GHz (36 $\sim$ 39 GHz) and the dual-band 3-dB axial ratios of 6% (27.3–29 GHz) and 8.4% (35–38.2 GHz) operates in both the RHCP and LHCP modes. The experimental result shows that the proposed antenna has a circular polarization bandwidth at the central frequencies of 28 and 38 GHz for both the RHCP and LHCP.

## 1. INTRODUCTION

The progress of mobile technology in support of many services has accelerated. This means that users of smart phones require higher data rates and bandwidths. Due to the increasing number of smart phone users, the demand for capacity has also risen. Some technologies are available to meet this huge need for capacity, such as massive multi-input and multi-output (MIMO), big data, the internet of things (IoT), and millimeter wave (mmWave) [1]. The most appropriate technology is to use the mmWave spectrum, because it has advantages including a large available bandwidth (BW) and vacant spectrum frequency [2]. The 5th generation (5G) mmWave mobile system is a candidate likely to increase communication capacity as required [3–5].

The 5G technology works with a packet switched wireless system, which covers a wide area and has a wide spectrum and high data rates. This cellular system will support uniform 0.1 to 1 Gbps data through a range of situations [5, 6]. It requires the 5G antenna to demonstrate applicable gain at the licensed mmWave frequencies of 28, 38, and 60 GHz, with a bandwidth around 1 GHz according to the U.S. Federal Communications Commission [7]. Furthermore, it can provide more attractive features and efficiency for users. However, even a small handset should manage such a complex collection of technological features.

In recent studies, circular polarization reconfigurable antennas have attracted more attention for their inherent characteristics such as multipath fading mitigation, phase fluctuation due to weather, and superior mobility [8–11]. Furthermore, these antennas have diverse polarization and can switch to right/left hand circular polarization (RHCP and LHCP), two horizontal and vertical linear polarizations, and elliptical polarizations [11–13]. Several circularly polarized antennas have been recommended for

*Received 30 May 2020, Accepted 28 August 2020, Scheduled 6 September 2020*
* Corresponding author: Nazih Khaddaj Mallat (nazih.mallat@aau.ac.ae).
[1] College of Engineering, Al Ain University, United Arab Emirates (UAE). [2] Department of Electrical Engineering, Sharif University of Technology, Iran. [3] Department of Computer & Electrical Engineering and Computer Science, Florida Atlantic University, USA. [4] College of Information Technology, UAE University, United Arab Emirates (UAE). [5] Department of Electrical Engineering, Arak University of Technology, Iran.

operation in 5G mobile systems [14–17]. The weakness of these antennas is static on the type of circular polarization. Other researchers have reported other mmWave areas with narrow BW and multiple feeding ports [18, 19]. Furthermore, the gain of the antenna can increase if one kind of lens is inserted, such as the one hemispherical lens produced from the dielectric material in front of it [20].

To meet the objectives of low profile structure, wide BW, simplicity, high isolation, reconfigurable polarization, and switchable RHCP and LHCP, this study proposes a novel 5G antenna. It operates at 28 GHz and is simple in structure; it could be appropriate for 5G mobile devices or a base station (BS) where space is limited. The paper reports the simulation of the proposed antenna structure by a high frequency structure simulator (HFSS), and then the result of the fabricated antenna is illustrated.

## 2. DESIGN GEOMETRY AND ANALYSIS

The optimized geometry and dimensions of the proposed 5G antenna are shown in Figure 1 and Table 1, respectively. The ground plane has a rectangular form with dimensions of $L \times W$. Two trapezoidal shapes and two symmetric curved shapes are derived from the ground plane. The substrate of prototypes is produced by Rogers RT/Duroid$^{TM}$ 5880 material with the following characteristics: $\varepsilon_r = 2.2$, $h = 0.8$ mm, and $\tan\delta = 0.0009$. The antenna structure can be divided into three parts:

- In the single slot of the coplanar waveguide (CPW), two rectangular slots are added in the slot by an optimized width to yield 50 Ω impedance for antenna feeding.
- The current path can be controlled by two PIN diodes in the upper strips. A DC voltage supply is used to feed these diodes through two stubs. The capacitor of each stub is around 0.17 pF, and when the two diodes are switched ON, these stubs act as a feed line.
- The performance of the proposed reconfigurable 5G antenna is essentially based on the two trapezoidal shapes and the two symmetric curved shapes on the ground plane.

**Table 1.** Optimized sizes of the proposed 5G-CP antenna.

| Parameter | Value (mm) | Parameter | Value (mm) |
|---|---|---|---|
| $L$ | 19 | $W$ | 17 |
| $l_1$ | 3.45 | $w_1$ | 1.23 |
| $l_2$ | 0.8 | $w_2$ | 1.75 |
| $l_3$ | 6.05 | $w_3$ | 1.95 |
| $l_4$ | 4.05 | $w_4$ | 1.72 |
| $l_5$ | 0.25 | $w_5$ | 1 |
| $l_6$ | 0.25 | $w_6$ | 6.15 |
| $l_7$ | 1.85 | $w_7$ | 2.7 |
| $l_8$ | 3.5 | $w_8$ | 1.35 |
| $g_1$ | 0.1 | $g_3$ | 0.25 |
| $g_2$ | 0.12 | $r$ | 2.9 |

The width of the CPW slot is approximately $\lambda_c/2$ at working frequency $f_c$ for all resonance frequencies. In order to excite linear polarizations, a CPW feed slot is designed. Two PIN diodes are employed to control the setup modes of the ground plane. These diodes are fed by a DC voltage supply through two stubs $1.35 \times 0.25$ mm [21] in size. The operational modes of short circuit (ON mode) and open circuit (OFF mode) equivalent transmission line models are presented in Figure 2(a) and Figure 2(b). The 2D structures in HFSS can be modeled via a Lumped RLC boundary [22].

When the diode is ON, the equivalent circuit contains a series structure of two capacitors (for DC blocking), an inductor, and a resistor. Likewise, in the OFF mode, the equivalent circuit consists of a series structure of two capacitors (for DC blocking), an inductor, and a resistor parallel with a capacitor.

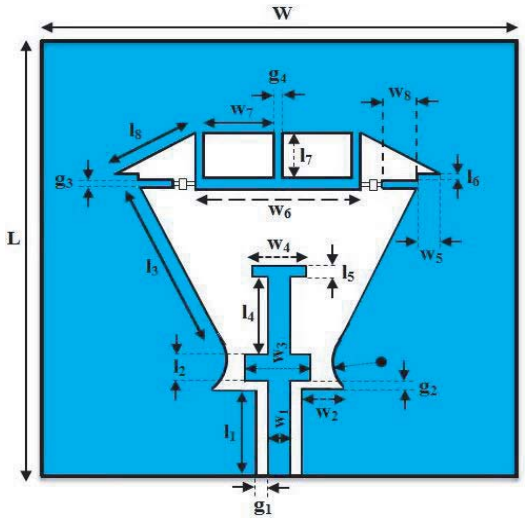


**Figure 1.** Prototype of the proposed 5G antenna..

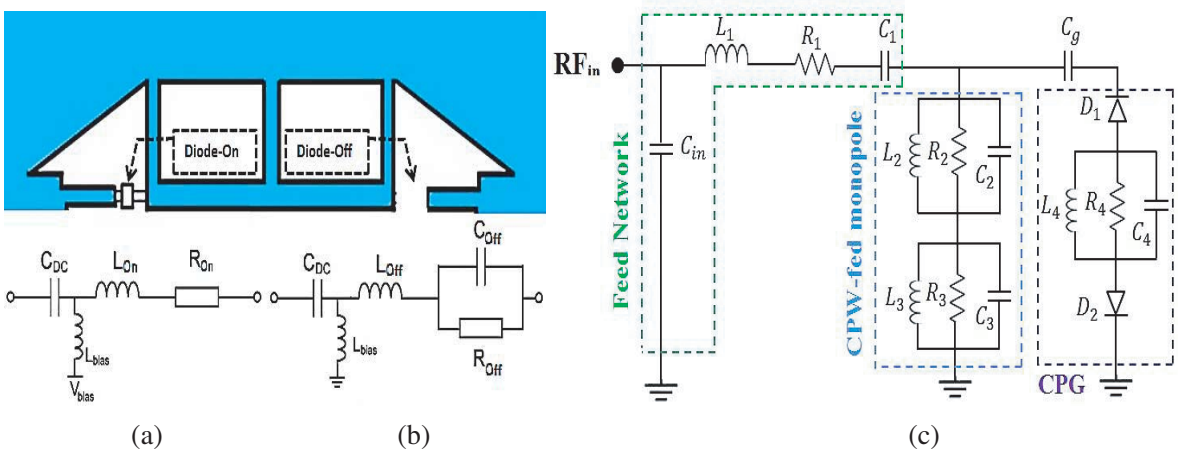


**Figure 2.** Equivalent circuit of transmission line model and PIN diode (a) ON mode, (b) OFF mode, (c) Equivalent circuit of the proposed 5G-CP antenna.

A MA4AGFCP910 PIN diode from MACOM is used for ON/OFF states in the proposed 5G-CP antenna to certify the RHCP and LHCP modes. The parameters of the equivalent circuits are collected in Table 2 for two ON/OFF modes based on the MA4AGFCP910 PIN diode. Please note that these values are achieved on 10 GHz frequency, and they are maximum possible values. On the other frequencies, these values are different. In fact, on 28 GHz frequency $C_{off}$ is three times smaller than 10 GHz. In addition, as described on the data sheet, by increasing $V_r$, amount of $Z_{off} = (\frac{1}{2\pi f_c C_{off}} || R_{off}) + 2\pi f_c L_{off}$ will increase. This amount for $V_r = 25$ mV is equal to 21 KΩ. Figure 2(c) shows the equivalent circuit of a transmission line model of the proposed 5G-CP antenna in three parts, namely the feed network, CPW-fed monopole, and CPG. The ON/OFF state of the PIN diodes is simulated by means of lumped RLC boundaries on HFSS. Due to operation mode (LHCP or RHCP), one of the diodes was on OFF mode, and the other one was on ON mode.

The proposed 5G antenna is fed by a 50 Ω K-connector on the CPW. This ground plane shape with two PIN diodes at the edge of trapezoidal shapes makes the CP achievable. Two sides of the PIN diodes are strips, which are separated by these diodes. When the right PIN diode is switched ON and the left one switched OFF, the polarization of the antenna will be RHCP, and conversely, the polarization of

**Table 2.** Equivalent circuit components of the PIN diode in the 5G bands.

| ON Mode | Value | OFF Mode | Value |
|---|---|---|---|
| $\boldsymbol{C_{DC}}$ | 2 pF | $\boldsymbol{C_{DC}}$ | 2 pF |
| $\boldsymbol{R_{On}}$ | 5.2 Ω | $\boldsymbol{R_{Off}}$ | 150 KΩ |
| $\boldsymbol{L_{On}}$ | 0.01 nH | $\boldsymbol{L_{Off}}$ | 0.01 nH |
| $\boldsymbol{C_{On}}$ | - | $\boldsymbol{C_{Off}}$ | 0.02 pF |
| $\boldsymbol{V}_{\text{bias}}$ | 1.4 V | $\boldsymbol{V}_{\text{bias}}$ | 0 V |

the 5G antenna will be LHCP.

Clearly, then, changing the modes of diodes changes the polarization. The theoretical analysis is concatenated into three parts, that is, the feed network, CPW-feed, and CPG. The equivalent circuit model of each part is calculated accurately on the lines of the theoretical method. The operational modes of RHCP and LHCP transition and equivalent transmission line models are displayed in Figure 2. In the RHCP mode, modes $D_1$ and $D_2$ are the On and Off modes, respectively. Therefore, in order to calculate $Z_{in}^{RHCP}$, $D_1$ and $D_2$ should be considered as equivalent circuits in Figure 2(a) and Figure 2(b), respectively. From Figure 2(c) the input impedance of CPG is formulated as follows:

$$\begin{cases} Z_1 = \left( j2\pi f_c L_{off} + \left( R_{off} \,||\, \dfrac{1}{j2\pi f_c C_{off}} \right) \right) \\ Z_2 = (Z_1 \,||\, j2\pi f_c L_{bias}) \\ Z_3 = \left( j2\pi f_c L_4 \,||R_4\,||\, \dfrac{1}{j2\pi f_c C_4} \right) \\ Z_4 = Z_3 + Z_2 + \dfrac{1}{j2\pi f_c C_{DC}} + R_{on} + j2\pi f_c L_{on} \\ Z_5 = (Z_4 \,||\, j2\pi f_c L_{bias}) \end{cases} \tag{1}$$

$$Z_{CPG}^{RHCP} = \left( Z_5 + \frac{1}{j2\pi f_c C_{DC}} \right) \tag{2}$$

where $Z_1$ is the impedance related to $D_2$ in the off mode, and then parallel with $L_{bias}$ which equals $Z_2$. $Z_3$ and $Z_4$ show the ground plane impedance and the impedance of serial $D_1$, $Z_3$, $Z_2$ in the CPG branch with $D_1$ in the on mode. Finally, $Z_{CPG}^{RHCP}$ checks the total impedance of this branch. $C_g$ is added to check the coupling between the monopole feed line and CPG.

$$Z_6 = \left( Z_{CPG}^{RHCP} + \frac{1}{j2\pi f_c C_g} \right) \tag{3}$$

The impedance of the CPW-fed line monopole consists of two series impedances, $Z_7$ and $Z_8$. The impedance of the CPW-fed line monopole is formulated as follows:

$$\begin{cases} Z_7 = \left( j2\pi f_c L_3 \,||\, R_3 \,||\, \dfrac{1}{j2\pi f_c C_3} \right) \\ Z_8 = \left( j2\pi f_c L_2 \,||\, R_2 \,||\, \dfrac{1}{j2\pi f_c C_2} \right) \\ Z_9 = Z_7 + Z_8 \end{cases} \tag{4}$$

The feed network consists of three series impedances including $j2\pi f_c L_1$, $R_1$, and $\frac{1}{j2\pi f_c C_1}$ and a parallel impedance, $\frac{1}{j2\pi f_c C_{in}}$ which represents the parasitic capacitance. The serial part of feed network is formulated as follows:

$$Z_{10} = j2\pi f_c L_1 + R_1 + \frac{1}{j2\pi f_c C_1} \tag{5}$$

The final input impedance of the RHCP mode is defined as:

$$Z_{in}^{RHCP} = ((Z_6||Z_9) + Z_{10})||\frac{1}{j2\pi f_c C_{in}} \tag{6}$$

In the LHCP mode, modes $D_1$ and $D_2$ are in the Off and On modes, respectively. Therefore, in order to calculate $Z_{in}^{lHCP}$ $D_1$ and $D_2$ should be considered equivalent circuits in Figure 2(b) and Figure 2(a), respectively. $Z_9$ and $Z_9$ have the same value in the RHCP mode. However, $Z_{CPG}$ will be changed.

$$\begin{cases} Z_{11} = (j2\pi f_c L_{on} + R_{on})|| j2\pi f_c L_{bias} \\ Z_{12} = Z_{11} + \dfrac{1}{j2\pi f_c C_{DC}} + Z_3 + Z_1 \\ Z_{13} = (Z_{12} \,||\, j2\pi f_c L_{bias}) \end{cases} \tag{7}$$

$$Z_{CPG}^{LHCP} = \left(Z_{13} + \frac{1}{j2\pi f_c C_{DC}}\right) \tag{8}$$

$$Z_{14} = \left(Z_{CPG}^{LHCP} + \frac{1}{j2\pi f_c C_g}\right) \tag{9}$$

The input impedance of the LHCP mode is formulated as:

$$Z_{in}^{LHCP} = ((Z_{14}||Z_9) + Z_{10})||\frac{1}{j2\pi f_c C_{in}} \tag{10}$$

The resonance accrues when the imaginary part of the input impedance becomes zero $\{w_0|\text{Imag}\{Z_{in}(w_0)\} = 0\}$. The capacitance of a microstrip line is assumed per length unit with a width of $w$ and a substrate thickness of $h$. The substrate permittivity of $\varepsilon_r$ is defined as follows [23]:

$$C = \begin{cases} \dfrac{\varepsilon_e}{60 \cdot c \cdot \ln\left(\dfrac{8 \cdot h}{W} + \dfrac{w}{4 \cdot \hbar}\right)} & \dfrac{w}{h} \leq 1 \\ \varepsilon_0 \varepsilon_e \left\{\dfrac{w}{h} + 2.42 - 0.44\dfrac{h}{w} + \left(1 - \dfrac{h}{w}\right)^6\right\} & \dfrac{w}{h} \geq 1 \end{cases} \tag{11}$$

In the circularly polarized mode, $h$ should be consumed as double the dielectric thickness. $c$ is the speed of light. $\varepsilon_e$ and $\varepsilon_0$ are the effective permittivity of the substrate and the permittivity of free air, respectively. $\varepsilon_0$ is equal to $\frac{10^{-9}}{36 \cdot \pi}$ [24]. $\varepsilon_e$ is defined as:

$$\varepsilon_e = \frac{\varepsilon_r + 1}{2} + \frac{\varepsilon_r - 1}{2}\left(1 + \frac{12 \cdot h}{w}\right) \tag{12}$$

Resistance and conductance per unit of length of a microstrip line are formulated as $R = 2 \cdot \alpha_c \cdot Z_0$ and $G = \frac{2 \cdot \alpha_d}{Z_0}$, respectively. $\alpha_c$ and $\alpha_d$ are the losses of conductor and dielectric, respectively. $Z_0$ is the characteristic impedance of the microstrip line. In this work $Z_0$ is considered $50\,\Omega$. At the MMW band, $G$ has small value and is negligible [23, 24]. The inductance of the microstrip line is defined as:

$$L = \frac{1}{jw}\left(Z_0^2\,(G + jwC) - R\right) \tag{13}$$

$C_g$ is defined as [23]:

$$C_g = \frac{-(C_4 + C_{CPW}) + \sqrt{(C_4 + C_{CPW})^2 - 4C_4 C_{CPW}(1 - C_c^{-2})}}{2} \tag{14}$$

$C_{CPW}$ shows the capacitance of the CPW-fed monopole line. $C_c$ is the coupling coefficient between two networks and is defined as $C_c = \frac{1}{\sqrt{Q_1 Q_2}}$. $Q_1$ and $Q_2$ are the quality factors of the CPW-fed monopole and CPG, respectively. The reflection coefficient is defined as follows [24]:

$$\Gamma = \frac{Z_{in} - Z_0}{Z_{in} + Z_0} \tag{15}$$

**Table 3.** Optimized parameters of the equivalent circuit.

| $C_1$ | $C_2$ | $C_3$ | $C_4$ | $C_g$ |
|---|---|---|---|---|
| 0.5 pF | 1.69 pF | 2.75 pF | 31.4 pF | 0.13 pF |
| $L_1$ | $L_2$ | $L_3$ | $L_4$ | |
| 0.064 nH | 4.21 nH | 6.8 nH | 78.4 nH | |
| $R_1$ | $R_2$ | $R_3$ | $R_4$ | |
| 50 Ω | 1.92 Ω | 5.3 Ω | 16 Ω | |

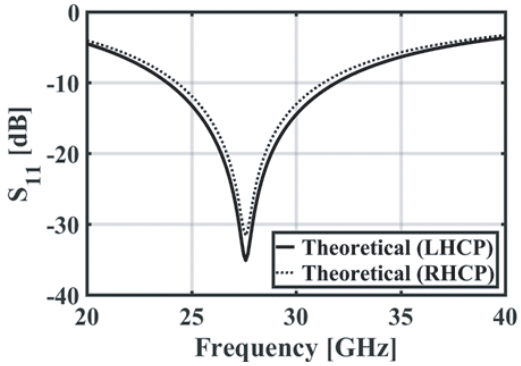


**Figure 3.** Theoretical $S$-parameter of the proposed 5G-CP antenna on LHCP and RHCP modes.

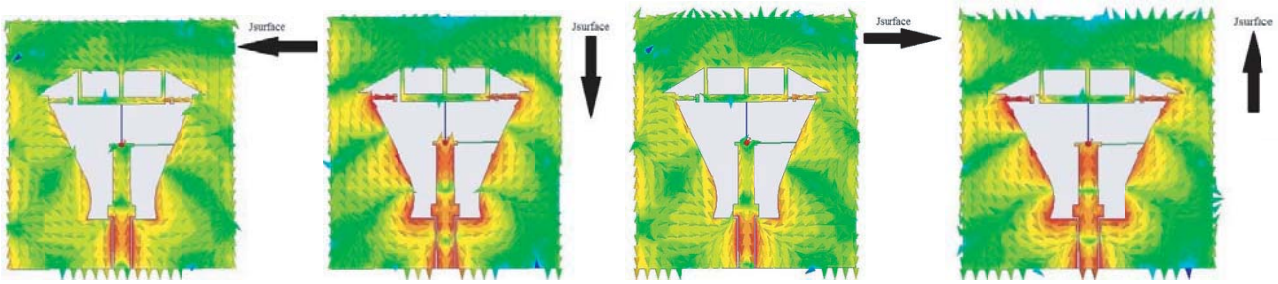


**Figure 4.** Simulated $J_{\text{surface}}$ distribution for different time-slots at 28 GHz (a) $t = 0$, (b) $t = T/4$, (c) $t = T/2$, (d) $t = 3T/4$.

With reference to Eq. (15), return loss is defined as $S_{11} = 20\log(\Gamma)$. The optimized values of equivalent circuit parameters are given in Table 3.

Figure 3 demonstrates the equivalent circuit response of the proposed 5G-CP antenna, for LHCP and RHCP modes, which resonates at a frequency of 27.5 GHz with a wide impedance bandwidth. Therefore, the proposed antenna can be expected to operate in the 5G band. The values of the parameters in Figure 1 are determined with reference to Eqs. (11) and (13). The length of the stubs in the ground plane of the antenna is modified to secure an appropriate match. An Ansoft HFSS is used for optimizing the antenna design and numerical evaluations [22]. The simulated surface current distribution $J_{\text{surface}}$ in the ground plane for the two modes can be observed in Figure 4. In this figure, the time slots $\{0, T/4, T/2, 3T/4\}$are shown at 28 GHz. It can be seen that the surface current of the ground plane circulates as time elapses due to the CP wave in the proposed antenna.

## 3. SIMULATION, MEASUREMENT AND DISCUSSION

In this section, the merits of the proposed 5G-CP antenna are investigated by the simulation and measurement results. First, the $S_{11}$ parameters of the antenna in different situations are illustrated. Second, to indicate the performance of the proposed antenna, the gain parameter is shown. The radiation patterns of the antenna in $E$-plane and $H$-plane for two operating bands are described in the next section. Finally, the performance of the proposed 5G-CP antenna, with the most recent suggested designs, is explored in Table 2. The fabricated model of the proposed 5G-CP antenna is shown in Figure 5. The bias network on the back plane for isolating the DC and RF signals can be seen.

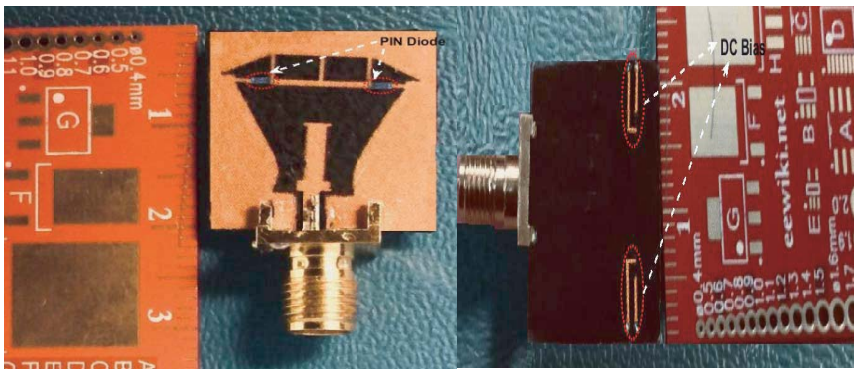


(a) (b)

**Figure 5.** The fabricated model of the proposed 5G-CP antenna: (a) Front; (b) Back.

### 3.1. Reflection Coefficient

To measure the $S_{11}$ parameters, an MS46122A vector network analyser is used. Then radiation patterns and realized gains are measured in an anechoic chamber, and the antenna is excited by a 50 Ω connector on the microstrip line. Figure 6(a) specifies that the proposed 5G-CP antenna has a simulated and measured impedance bandwidths ($|S_{11}| < 10$ dB) about 2.5 GHz ranging from 27 to 29.5 GHz, and about 3 GHz from 36 to 39 GHz with impedance BW (IBW $= \frac{\Delta f}{f_c}$) of 9 percent and 7.8 percent, respectively. It can be seen that both licensed bands (28 and 38 GHz) are supported by the proposed 5G-CP antenna.

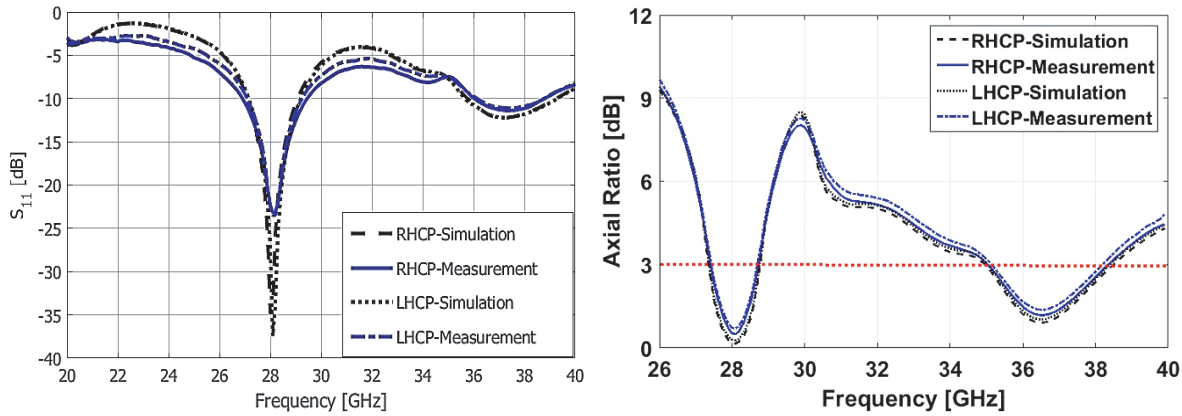


(a) (b)

**Figure 6.** Simulation and measurement $S$-parameter and axial ratio parameter of the proposed 5G-CP antenna: (a) $S_{11}$; (b) Axial ratio.

The axial ratio (AR) of the 5G-CP antenna versus frequency is presented in Figure 6(b). The axial ratio of the proposed CP antenna is measured based on technique proposed in [30]. This technique has high accuracy. It should be mentioned that the proposed 5G-CP antenna displays a dual-band 3-dB AR of 6% (27.3–29 GHz) and 8.4% (35–38.2 GHz). Furthermore, it makes two minimum points with values of 0.25 dB and 1.2 dB close to 28 GHz and 36.7 GHz, respectively.

An optimized structure design is obtained by changing the structural elements to match the appropriate impedance and radiation pattern. The two key structural elements, which have major roles in the operating performance of the proposed antenna, are investigated in this section. By changing these two parameters, other countries' licensed 5G bands, which have lower frequencies than FCC, can be supported. These parameters can be defined as:

- Length of CPW and ground gap ($g_l$).
- Length of upper rectangle of CPW ($l_5$).

The effect of increasing the $g_1$ parameter on the $S_{11}$ performance of the antenna is illustrated in Figure 7(a). It should be noted that changing the gap length enhances the impedance bandwidth especially in the 38 GHz band and shifts the resonance frequency to the higher bands. A lower amount of $g_1$ shifts the resonance frequency to the lower frequency band and to a smaller impedance bandwidth in the operating bands. Contrariwise, this parameter can also disturb the released gain of the proposed antenna. The $S_{11}$ response demonstrated in Figure 7(b) depicts the impact of the length of the upper rectangle of CPW ($l_5$) on the performance of the proposed antenna. This parameter has a converse impact on the resonance frequency and the impedance bandwidth. A higher value of $l_5$ shifts the resonance frequency to the lower bands, improves the matching, and reduces the impedance bandwidth. In some higher values of $l_5$, the antenna switches to a multiple-band state.

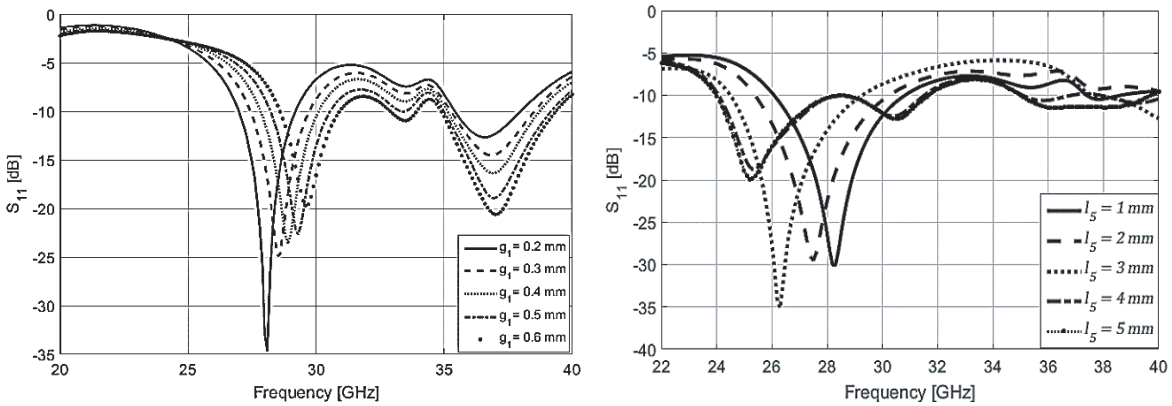


**Figure 7.** Effects of length $g_1$ and $l_5$ parameters on the $S_{11}$ performance of the proposed 5G-CP antenna: (a) $g_1$; (b) $l_5$.

### 3.2. Released Gain and Radiation Efficiency

The simulation and measurement peak gains for RHCP and LHCP modes are compared through the 5G-mmWave frequencies of interest in Figure 8(a). It is plain that the two graphs in any mode are well matched with a maximum reduction of 0.9 dB in the gain due to the misalignment of the connector (loss around 0.5 dB), a small mistake in production and other losses (loss around 0.4 dB). The proposed 5G-CP antenna shows maximum gain at about 8.7 dBi (measured) in the 28 GHz band and 8 dBi in the 38 GHz band. Furthermore, the gain decreases to around 4.5 dB in the frequency bands that are not of interest. In Figure 8(b), the simulated radiation efficiency of the proposed 5G-CP antenna is also displayed. The two peak efficiencies of 90.1% and 82.3% at the frequencies 28.5, and 37 GHz can be observed in the RHCP mode. Similarly, in the LHCP mode, two peak efficiencies of 88.3% and 79.6% at the frequencies 29 and 37 GHz can be observed for the RHCP mode. The radiation patterns of the

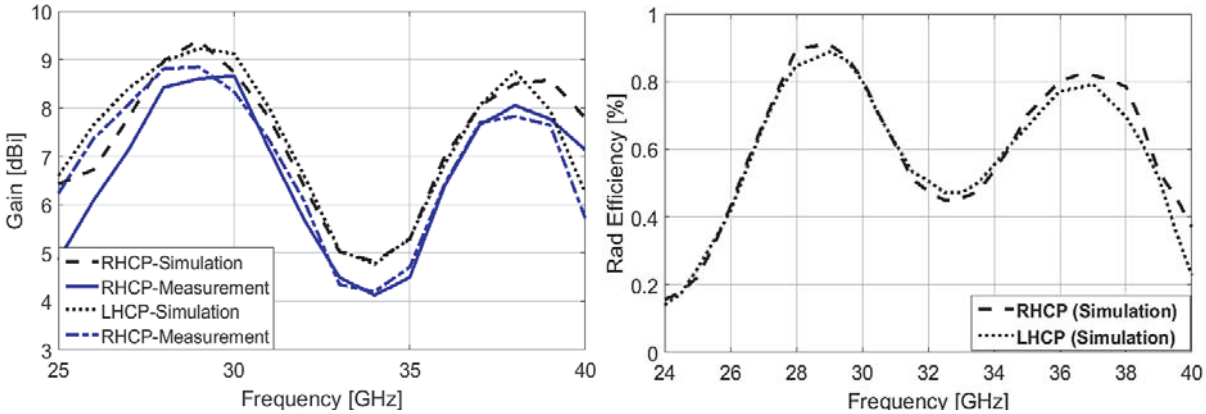


(a) (b)

**Figure 8.** Comparison of simulation and measurement gain and radiation efficiency of the proposed 5G-CP antenna for RHCP and LHCP modes: (a) Gain; (b) Radiation efficiency.

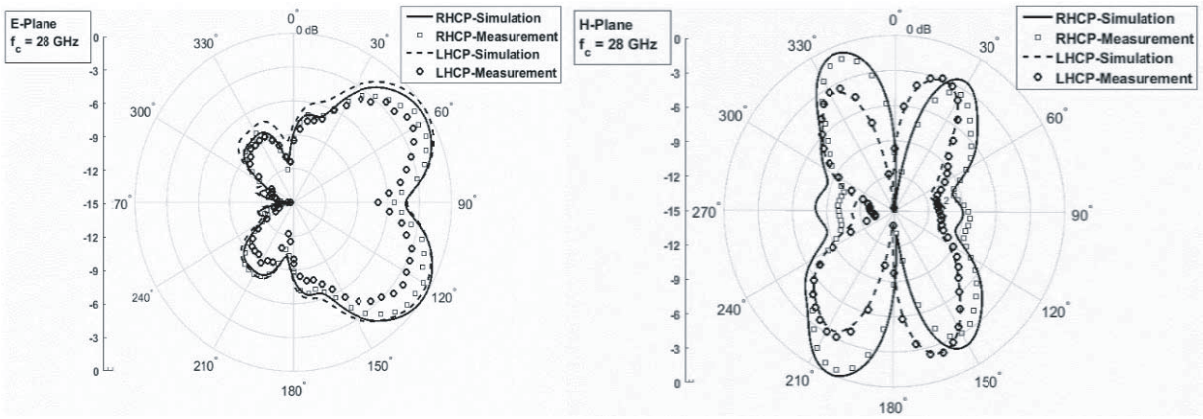


(a) (b)

**Figure 9.** Simulation and measurement normalized radiation patterns for RHCP and LHCP at 28 GHz: (a) $E$-Plane; (b) $H$-Plane.

proposed antenna are obtained by the two RHCP and LHCP polarizations in the operating bands of 28 and 38 GHz in Figure 9 and Figure 10, respectively. Pattern measurement setup is based on the pattern measurement technique proposed in [31]. By changing the mode of antenna from RHCP to LHCP or vice versa, the direction of antenna beam will be changed. However, as it is obvious from Figure 8, the maximum gains of antennas on the LHCP and RHCP modes have a small difference. This difference is less than 1.2 dB for 25–40 GHz frequency band. Furthermore, all the graphic numbers are revised and corrected. All the radiation patterns have been normalized to their minimum amount.

An appropriate match can be observed between the simulation results for HFSS and the measurement ones. The reduction in the measurement results in comparison to the simulation results is related to the misalignment of the connector and the antenna production. Two beam directional radiations are attained on the $E$-plane and $H$-plane with asymmetric shapes due to ON-OFF PIN diode modes. In Figure 9, the 3 dB beamwidths for the frequency of 28 GHz in the $E$-plane are around 50° (from 30° to 80°) with the maximum gain of 9.5 dBi, while the maximum 3 dB beamwidths in the $H$-plane are around 30° (from 190°–220°) with the maximum gain 2 dBi. In Figure 10, the 3 dB beamwidths for the frequency 38 GHz in the $E$-plane are around 90° (from 45° to 135°) with the maximum gain 8.3 dBi, while they are around 40° (from 45° to 135°) with the maximum gain of 1.9 dBi in the $H$-plane.

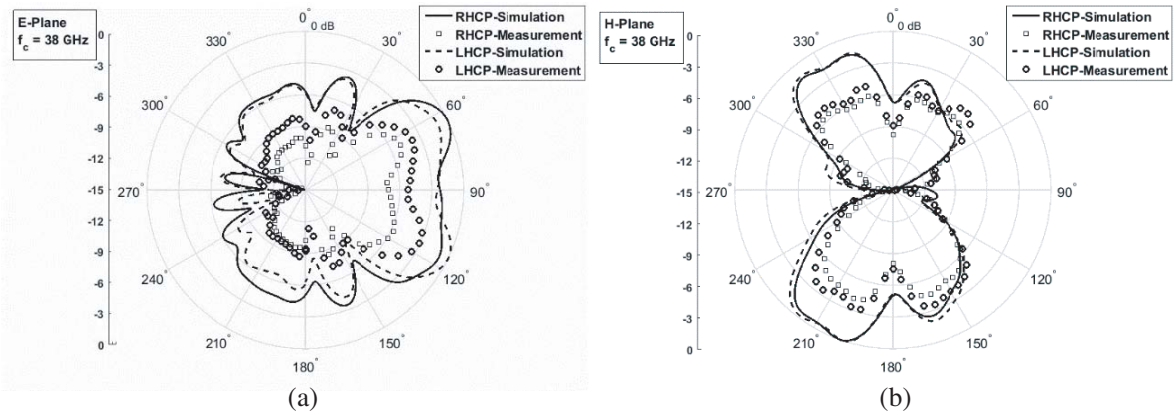


(a) (b)

**Figure 10.** Simulation and measurement normalized radiation patterns for RHCP and LHCP at 38 GHz: (a) $E$-Plane; (b) $H$-Plane.

## 4. PERFORMANCE COMPARISON

Table 4 reports the comparison between the performance characteristics of some recent reported mmWave-CP designs and the proposed antennas. The switchable polarization between LHCP and RHCP can be achieved [25, 26]. In [25], the design is large in size, with 8 switches inside, a lower IBW and gain than our proposed design can offer. The authors in [26] proposed a simply structured design with two diodes, but one with low IBW and gain compared to our proposed design. Although the proposed antenna in [27] has a wide tuning frequency range, the gain is not high enough in the 5G-mmWave bands. The proposed 5G-CP antenna has a compact form, unlike those described in other recent papers. The proposed design needs two PIN diodes to switch the polarization between LHCP and RHCP. It achieves higher gain and appropriate IBW. The authors in [28] proposed a broadband 5G-CP antenna that exhibits high gain. However, it has three dimensions and is not compact. Another example is that in [29] the authors designed a 5G-CP antenna of small dimension, dual bands, and high radiation efficiency. The disadvantage of this antenna was its low gain in operating bands, which limits its industrial applications.

**Table 4.** Comparison of recent reported designs with proposed 5G-CP antennas.

| Design | $f_0$ (GHz) | Total Dim. ($mm^3$) | Relative Dim. | $G_{max}$ (dBi) | $\delta G$ (dB) | FCC | ETSI | Radiation eciency (%) | E-plane 3-dB BW | H-plane 3-dB BW | IBW (%) | No. Band | $R_e$ (%) |
|---|---|---|---|---|---|---|---|---|---|---|---|---|---|
| [25] | 28 | 4.4 × 1.8 × 1.52 (single element) | 0.04 | 7.3 | not shown | ✓ | - | - | - | - | 3.47 | 1 | 90 |
| [26] | 28 | 11.6 × 6 × 0.254 | 0.07 | 7.2 | not shown | ✓ | ✓ | - | $83^o$ | $100^o$ | 3.52 | 1 | - |
| [27] | 38 | 10.5 × 6 × 3 (single element) | 0.73 | 7.2 | < 3 | ✓ | ✓ | - | - | - | 23.6 | 1 | 52 |
| [28] | 28 | 10 × 10 × 7.605 | 2.94 | 14.1 | < 1.8 | ✓ | ✓ | - | - | - | 27.6 | 1 | - |
| [29] | 24<br>28.5 | 2.7 × 3.2 × 1.52 | 0.05 | 3.5–4 | 2.5 | ✓ | ✓ | > 70 | - | - | 4.1–15.8 | 2 | 92–95 |
| Our design | 28<br>38 | 19 × 17 × 0.8 | 1 | 9.4 | < 1.8 | ✓ | ✓ | > 80 | $50^o$<br>$90^o$ | $30^o$<br>$40^o$ | 9–7.8 | 2 | 90–79 |

## 5. CONCLUSION

A novel reconfigurable polarization patch antenna is proposed in this paper, with theoretical discussion and verification for the upcoming 5G mobile systems. The proposed design has a switchable ground plane using two independent PIN diodes which produce two polarizations, RHCP and LHCP. This antenna can achieve two orthogonal polarizations by changing the PIN diode modes, and it has the advantages of compactness and easy fabrication. The simulation and measurement results demonstrate that the proposed 5G-CP antenna has a well-matched IBW from 27 to 29.5 GHz and 36 to 39 GHz, and a dual-band 3-dB AR of 6% (27.3–29 GHz) and 8.4% (35–38.2 GHz) for each polarization. The measured gain of the proposed antenna is greater than 9 and 7.8 dBi.

## REFERENCES

1. Akyildiz, F., et al., "5G roadmap: 10 key enabling technologies," *Computer Networks*, Vol. 106, 17–48, 2016.
2. Haraz, O. M., "Broadband and 28/38-GHz dual-band printed monopole/elliptical slot ring antennas for the future 5G cellular communications," *J. Infrared Milli Terahz Waves*, Vol. 37, 308–317, 2016.
3. Li, Q. C., et al., "5G network capacity: Key elements and technologies," *IEEE Vehicular Technology Magazine*, Vol. 9, No. 1, 71–78, 2014.
4. El-Halwagy, W., et al., "Investigation of wideband substrate-integrated vertically-polarized electric dipole antenna and arrays for mmWave 5G mobile devices," *IEEE Access*, Vol. 6, 2145–2157, 2018.
5. Rappaport, T. S., et al., "Millimeter wave mobile communications for 5G cellular: It will work!," *IEEE Access*, Vol. 1, 335–349, 2013.
6. Wang, C. X., et al., "Cellular architecture and key technologies for 5G wireless communication networks," *IEEE Communications Magazine*, Vol. 52, No. 2, 122–130, 2014.
7. Register, F., "Use of spectrum bands above 24 GHz for mobile radio services," *Federal Communications Commission*, Vol. 81, No. 219, 2016.
8. Nishamol, M. S., et al., "An electronically reconfigurable microstrip antenna with switchable slots for polarization diversity," *IEEE Transactions on Antennas and Propagation*, Vol. 59, No. 9, 3424–3427, 2011.
9. Yang, X.-X., et al., "A polarization reconfigurable patch antenna with loop slots on the ground plane," *IEEE Transactions on Antennas and Propagation*, Vol. 1, 69–721, 2012.
10. Li, Y., et al., "Polarization reconfigurable slot antenna with a novel compact CPW-to-slotline transition for WLAN application," *IEEE Antennas and Wireless Propagation Letters*, Vol. 9, 252–255, 2010.
11. Pyo, S., J. Baik, and Y. Kim, "Slot-perturbed microstrip antenna for switchable circular polarisation," *Electronics Letters*, Vol. 47, No. 10, 583–585, 2011.
12. Lawrence, N. P., et al., "5G terrestrial networks: Mobility and coverage-solution in three dimensions," *IEEE Access*, Vol. 5, 8064–8093, 2017.
13. Wang, K. X. and H. Wong, "A circularly polarized antenna by using rotated-stair dielectric resonator," *IEEE Antennas and Wireless Propagation Letters*, Vol. 14, 787–790, 2015.
14. Bisharat, D. J., S. Liao, and Q. Xue, "High gain and low cost differentially fed circularly polarized planar aperture antenna for broadband millimeter-wave applications," *IEEE Transactions on Antennas and Propagation*, Vol. 64, 33–42, 2016.
15. Akbari, S. G. M., et al., "Analytic study on CP enhancement of millimeter wave DR and patch subarray antennas," *International Journal of RF and Microwave Computer-Aided Engineering*, Vol. 27, No. 1, e21053, 2017.
16. Park, S. J. and S. O. Park, "LHCP and RHCP substrate integrated waveguide antenna arrays for millimeter wave applications," *IEEE Antennas and Wireless Propagation Letters*, Vol. 16, 601–604, 2017.

17. Asaadi, M. and A. Sebak, "High-gain low-profile circularly polarized slotted SIW cavity antenna for mmWave applications," *IEEE Antennas and Wireless Propagation Letters*, Vol. 16, 752–755, 2017.
18. Guntupalli, A. B. and K. Wu, "Frequency-steered directive beam with dual circular polarization and two-dimensional scan capability for millimeter wave imaging and sensing systems," *IEEE WAMICON*, 1–3, 2014.
19. Cheng, Y. J., W. Hong, and K. Wu, "Millimeter wave half mode substrate integrated waveguide frequency scanning antenna with quadri-polarization," *IEEE Transactions on Antennas and Propagation*, Vol. 58, 1848–1855, 2010.
20. Haraz, O. M., "Millimeter-wave printed dipole array antenna loaded with a low-cost dielectric lens for high-gain applications," *J. Infrared Milli Terahz Waves*, Vol. 41, 225–244, 2020.
21. https:cdn.macom.com/datasheets/MA4AGP907-MA4AGFCP910.pdf.
22. Ansoft HFSS, Ver. 15, Ansoft Corporation, Pittsburgh, PA, 2015.
23. Kanaujia, B. K., M. K. Khandelwal, S. Dwari, S. Kumar, and A. K. Gautam, "Analysis and design of compact high gain microstrip patch antenna with defected ground structure for wireless applications," *Wireless Personal Communications*, Vol. 91, No. 2, 661–678, 2016.
24. Cheng, D. K., *Field and Wave Electromagnetics*, Pearson Education India, 1989.
25. Syrytsin, I., et al., "User effects on the circular polarization of 5G mobile terminal antennas," *IEEE Transactions on Antennas and Propagation*, Vol. 66, No. 9, 4906–4911, 2018.
26. Abbas, E. A., A. T. Mobashsher, and A. Abbosh, "Polarization reconfigurable antenna for 5G cellular networks operating at millimeter waves," *IEEE Asia Pacific Microwave Conference (APMC)*, 772–774, Kuala Lumpar, 2017.
27. Wu, Q., et al., "Millimeter wave multi beam endfire dual-circularly polarized antenna array for 5G wireless applications," *IEEE Transactions on Antennas and Propagation*, Vol. 66, No. 9, 4930–4935, 2018.
28. Hussain, N., M. Jeong, J. Park, and N. Kim, "A broadband circularly polarized fabry-perot resonant antenna using a single-layered PRS for 5G MIMO applications," *IEEE Access*, Vol. 7, 42897–42907, 2019.
29. Aboualalaa, M., et al., "Independent matching dual-band compact quarter-wave half-slot antenna for millimeter-wave applications," *IEEE Access*, Vol. 7, 130782–130790, 2019.
30. Li, B., Y. Deng, J. Zhang, and Z. Zhou, "Novel method for measuring the axial ratio of circularly polarized antennas based on the cross-polarization," *2017 Sixth Asia-Pacific Conference on Antennas and Propagation (APCAP)*, 1–3, IEEE, 2017.
31. Rodenbeck, C. T., K. Chang, and J. Aubin, "Automated pattern measurement for circularly-polarized antennas using the phase-amplitude method," *Microwave Journal*, Vol 47, No. 7, 2004.